Artificial, Photoinduced Activation of Nitrogenase Using Directed and Mediated Electron Transfer Processes

Matan Moshe Meirovich, Oren Bachar and Omer Yehezkeli

Technion, Israel Institute of Technology

Abstract

Nitrogenase, a bacteria-based enzyme, is the sole enzyme able to generate ammonia by atmospheric nitrogen fixation. Thus, improved understanding of its mechanism and developing methods to artificially activate it may contribute greatly to basic research, as well as to the design of future artificial systems. Here, we present methods to artificially activate nitrogenase using photoinduced reactions. Two nitrogenase variants originating from *Azotobecotor vinelinii* were examined using photoactivated CdS nanoparticles (NPs) capped with thioglycolic acid (TGA) or 2-mercaptoethanol (ME) ligands. The effect of methyl viologen (MV) as a redox mediator of hydrogen and ammonia generation was tested and analyzed. We further determined the NPs conductive band edges and their effect on nitrogenase photo-activation. The nano-bio hybrid systems comprising CdS NPs and nitrogenase were further imaged by transmission electron microscopy, confirming their formation for the first time. Our results show that the ME-capped CdS NPs–nitrogenase enzyme biohybrid system with added MV as redox mediator, leads to a five-fold increase in the production of ammonia compared with the non-mediated biohybrid system.

Introduction

Electrical communication between enzymes and their surroundings is tightly controlled by natural diffusional redox mediators.[1–5] Alternatively, protein-protein interactions at specific docking sites can force short electron transfer distances that, in turn, allow efficient electron transfer. The outer shells of redox enzymes are, by design, insulators and so prevent short circuits with undesired electron carriers present in surrounding proteins. In the last several decades, the theoretical and experimental foundations of these processes were developed, improving our understanding thereof. Establishing electrical communication between redox proteins and electrodes or inorganic nanomaterials is a major challenge that has been at the forefront of research for the last two decades. Using redox mediators or directed electron transfer configurations has led to a variety of sensing or energy generation devices.

For example, glucose oxidase (GOx) and glucose dehydrogenase (GDH) were each conjugated with electrodes and nanoparticles (NPs) for the development of amperometric glucose biosensors.[6–9] Photosystem I and Photosystem II proteins were each coupled to either electrodes to construct photo-bioelectrochemical cells or to Pt and Pd nanoclusters to generate hydrogen.[10–13] Hydrogenase was coupled to NPs or to an electrode, facilitating high turnover rates in both hydrogen oxidation and proton reduction reactions.[14–16] In all these examples, tailored chemistries for direct electron transfer processes or integration of redox mediators enabled enzyme activation. Several parameters should be taken into account when establishing electrical communication between biotic and abiotic materials: (i) short electron transfer distance, (ii) orientation of the proteins' active site with respect to the electron acceptor or donor, and (iii) adjusting the redox potential to allow the directional electron transfer process.

Nitrogenase, a bacteria-based enzyme with a $\alpha_2\beta_2\delta_4$ heterooctameric or $\alpha_2\beta_2$ heterotetramer composition (*Azotobacter vinelandii*, VFe-P, and MoFe-P, respectively), is the sole enzyme able to generate ammonia by atmospheric nitrogen fixation[17,18] Although these exceptional enzymes have been studied for several decades, their activation mechanism has yet to be fully resolved.

For example, nitrogenase was coupled to an electrochemical mediated system in order to reduce azide or CO_2 into NH_3 or H_2 / formate under highly biased electrodes.[19,20] By integrating a nitrogenase-based cathode with a hydrogenase-based anode, a biofuel cell mimicking the Haber-Bosch process was developed.[21,22] In most cases, cobaltocene was used as a redox mediator, hence a bias of -1.1V vs. Ag/AgCl was used for activation.

The nitrogenase αβ subunits consist of two metal centers: (i) The P-cluster, an iron-sulfur center (8Fe:7S), which acts as an electron mediator accepting the shuttled electrons from the Fe-protein; and (ii) the M-cluster, a unique complex with a 7Fe:9S:M:1C center, which acts as the catalytic center and allows N_2 fixation to occur. M represents molybdenum, vanadium or iron metal ions, and C represents carbide. Activation of nitrogenase requires Mg-ATP and reduced Fe-protein. The ATP allows a structural conformation change in the Fe-protein, leading to efficient electron transfer toward the P-cluster.[23] ATP does not act as an electron donor, and only supports the binding of the Fe-protein to the nitrogenase P-cluster. The mechanism of the process is not yet fully understood and methods to overcome the gated process should be developed. It is known that $8e^-$ are involved in the process, which produces two moles of NH_3 and one mole of H_2 as a by-product (see Eq. 1).

$$N_2 + 8e^- + 8H^+ \xrightarrow[16Mg\text{-}ATP]{} \xrightarrow[16Mg\text{-}ADP + 16Pi]{} 2NH_3 + H_2$$

Equation 1: *Nitrogen fixation process.*

It has been shown that nitrogenase can be activated by using CdS NRs, anchored $Ru(bpy)_3$, or pyrene moieties without the addition of ATPs and Fe-protein.[24–26] Although NH_3 production by MoFe-P is very attractive, several challenges limit further progress: (i) The MoFe-P redox-active sites, the P-cluster, and the M-cluster, are all extremely sensitive to the presence of oxygen; (ii) The MoFe-P electron transfer mechanism for NH_3 generation requires eight successive moles of electrons to generate two moles of NH_3. Furthermore, the reduction mechanism or the way in which the N_2 molecule coordinates with the M-cluster complex is not fully understood and is still under debate;[27,28] and (iii) In nature, electron transfers occur in eight consecutive steps of a single electron transfer toward the P-cluster, which thereafter transfers these electrons to the M-cluster. In this process, the reduced Fe-protein acts as an electron donor, while an ATP molecule functions as a kind of key that forces a structural change in the Fe-protein, thus allowing the electron transfer process. This rate-limiting process, which occurs in nature, may be improved and methods to bypass this regulated mechanism should be developed to allow artificial activation of nitrogenase enzyme by external stimuli or an electron source other than the Fe-protein. Several basic questions remaine unanswered: How does the interface between nitrogenase and the artificial system (electrode, NPs, etc.) influence the electron transfer process? How does the nitrogenase bind to the electrode or semiconductor?

As mentioned, artificial activation of nitrogenase has been recently realized, although the role of the Fe-protein or its absence in artificial systems, the electron transfer process, and the conditions affecting the ammonia and hydrogen generation remained unresolved and warrant further investigation.

Here, we show a direct and diffusional approach to the artificial activation of MoFe-P by CdS NPs 10 nm in diameter (see Fig. 1). We examined the role of different ligands and their effect on the direct electron transfer process, and then examined the mediated electron transfer process using methyl viologen (MV) as a redox mediator. The generated NH_3 was determined by an updated analytical method that minimizes the false-positive response that may occur when using the commonly used fluorescence-based probe.

Two variants of MoFe-P, which express a His-tag, were isolated from *Azotobacter vinnelenlii* mutated strains DJ1194 and DJ995 as previously described.[29,30] The mutated αL158C MoFe-P, isolated from DJ1194, consists of cysteine at the α158 instead of lysine as expressed in the wild type (WT MoFe-P). The close proximity of Cys α158 to the iron-sulfur P-cluster at the nitrogenase's electron acceptor site could potentially allow a short electron transfer distance between a bonded external electron donor and the enzyme's P-cluster. Indeed, Tzecan and co-workers showed methods of integrating $Ru(bpy)_3$-based photosensitizers with nitrogenase for independent Fe-protein activation. The artificial system was limited by photosensitizer degradation, preventing continuous long-term activation.[24]

For the artificial activation of nitrogenase, 10-nm CdS NPs were synthesized using a hydrothermal method.[31] The CdS particle size was determined using transmission electron microscopy (TEM) imaging and UV/Vis spectroscopy (Figs. 2a and 2b). Using ligand exchange steps, we altered the CdS NPs surface by replacing the oliel amine/oleic acid with shorter thioglycolic acid (TGA) or 2-mercaptoethanol (ME) ligands, (see Fig. S2). The CdS NPs were dissolved in aqueous solution and their charges were varified using gel electrophoresis and zeta potential measurements (Fig. 2c). As expected, the TGA-modified CdS NPs exhibited dominant-negative charges and traveled through the 0.6% agarose gel to the positive pole. On the other hand, the ME-modified CdS NPs showed only a minute effect and did not migrate from the well, although small negative charges were measured by the zeta potential setup. Ligands have an important effect on the energy levels or traps on the NPs' surface.[32–34] Since the position of the energy levels in the CdS NPs could greatly affect the photoinduced electron transfer process, we determined the band edges of CdS-TGA and CdS-ME NPs using capacitance measurements (Mott-Schottky technique).[35,36] The TGA form exhibited a Conductive band (CB) value of -0.9V vs. Ag/AgCl, pH 7.2 while the ME form exhibited a higher negative potential of -1.2V (Fig. 2d). As shown previously, thiol-Cd interactions form electrons or hole traps on the surface of NPs[32–34], which subsequently slow down recombination reactions and allow improved electron transfer processes. The TGA- and ME-modified CdS NPs were further utilized for photoinduced nitrogenase activation. In each experiment performed, oxygen-free CdS NPs (stored in an Ar-filled glove box, O_2<0.2 ppm) were mixed with phosphate buffer (PB) pH 7.2 and ascorbic acid, which was used as an electron donor. The sealed vial was then purged in the dark with N_2 for 1 hr followed by injection of the MoFe-P solution, in the glove box, using an insulin syringe (Pic solution, 0.5mL, 31G). Then, the sealed vails were irradiated using a 465-nm LED light. The H_2 generated was monitored using a GC-TCD and the NH_3 generation was determined using an o-phthaladehyde (OPA) fluorescence probe, which was later extracted to chloroform as depicted in Fig. S6. The NH_3 detection method was validated using NH_3 samples of known concentrations, as described in the supporting information. With this method, a detection limit of 5μM can be reached, (see Fig. S5). Using the developed method and GC-TCD chromatography, we examined how the charges on the NPs' ligands affect the biohybrid system activation. Figure 3 depicts the amounts of H_2 and NH_3 obtained using CdS NPs-MoFe-P mixtures. We examined two variants of the nitrogenase protein: WT MoFe-P (His-Tag, DJ995) and αL158C mutated nitrogenase (His-Tag, DJ1094). The cysteine-mutated nitrogenase potentially has two Cys positions that may directly bond the NPs through the strong thiol-Cd interaction. The mixtures of CdS-ME NPs with both of the nitrogenase variants generated double amounts of H_2 compared with the TGA NPs mixtures. We also observed that using αL158C MoFe-P, generated up to ~2000nmol of H_2 after only two hours of blue light irradiation. MV is a commonly used redox relay unit for both biotic and abiotic electron transfer processes[37–39]. The pH-independent one-electron reaction has a strong reducing potential of -0.67V vs. Ag/AgCl in aqueous

solutions, which can be used for MoFe-P P-cluster reduction (~-0.5V). MV was therefore introduced into the CdS-ME/TGA NPs-MoFe-P mixture, and H_2 and NH_3 generation was monitored. Interestingly, when MV was added to the mixture as an electron shuttle mediator, H_2 generation was completely inhibited. By measuring the extracted NH_3–OPA conjugates without the presence of MV, both MoFe-P variants produced similar amounts of NH_3 regardless of the capping ligands. On the other hand, adding MV to the CdS-TGA NPs led to a two-fold increase in the amounts of NH_3 generated compared with the MV-free reactions. Moreover, when WT MoFe-P and αL158C MoFe-P were activated with CdS-ME NPs, a five-fold increase in NH_3 production was observed. We further tracked the rate of NH_3 generation (Fig. S8) and recorded similar rates of 0.1 nmol/min for both variants activated by CdS-ME NPs in the presence of MV. In our design, we assume electrostatic interactions between CdS NPs and MoFe-P. To examine this hypothesis, we examined the nano-biohybrid system using TEM imaging. Samples were stained with uranyl acetate to allow nitrogenase imaging, which demonstrated the formation of nano-biohybrids of nitrogenase and the CdS-ME NPs (red arrows in Figs. 4 and S10).

Discussion

The results obtained indicate that the addition of MV can enhance the amount of NH_3 generated compared with nitrogenase that is activated solely by CdS NPs. Moreover, the results show that ME-capped NPs lead to better catalytic performance compared with the charged TGA ligand. To better understand this phenomenon, we first examined the CB edges of the capped NPs (Fig. 2d). The CB edge of CdS-ME NPs is ~300mV more negative than that of CdS-TGA NPs. As the data reveals, we can exclude the option of direct N_2 reduction by the CdS NPs surface with or without MV as redox mediator or catalyst. We also examined whether chemically reduced MV can contribute directly to nitrogenase activation, and found that NH_3 generation was low (Fig. S9). The data obtained suggest that the CdS surface is essential for the reduction process, and that MV dramatically increases process efficiency. This might be as a result of a conformational change in the nitrogenase proteins that allows better electron injection into the nitrogenase P-cluster. The ME ligand has two different roles in the catalytic process: (i) it shifts the CB potential to -1.2V (vs. Ag/AgCl), and (ii) it weakens the electrostatic interaction with MV and/or the MoFe-P. Analysis of the result obtained without MV leads us to conclude that the CB potential has only a minute effect and we can, therefore, suggest that the less prominent charges of the ME ligands enable improved release of mediator leading to higher turnover rates. The αL158C MoFe-P consists of two Cys sites that can potentially bond directly to NPs. If indeed the conjugation occurs at the Cys 158 site, an improved electron transfer rate should be expected. By comparing the results obtained with αL158C MoFe-P and with WT MoFe-P, we can conclude that no direct integration occurs or that it may shift the catalytic process to prefer a hydrogenation mechanism that minimizes N_2 fixation. The enhanced amount of H_2 obtained with αL158C

MoFe-P could indicate the latter. It should be noted that when MV is introduced into the system, H_2 cannot be measured; Although MV is a well-known electron transfer carrier, it does not transfer protons. It is possible that the protein's natural activity is prohibited and that the fast electron injection caused by MV eliminates H_2 generation and drives solely to ammonia production. It has been shown that the Fe protein binds to nitrogenase via a positively charged docking site.[40–42] We hypothesized that TGA-CdS NPs with negative charges on their surface will bind to the docking site and force improved electron transfer process. By examining the obtained data (Fig. 3), we conclude that such an effect did not occur. While surface charges can enable electrostatic interactions between NPs and MoFe-P, they cannot force the gated conformational changes required to allow the electron transfer process; this key process must be controlled for improved activity. Examining the TEM imaging (Figs. 4 and S10), it is clear that at least one αL158C nitrogenase is bonded to each ME-CdS NP. These results confirm that although conjugation is indeed achieved, it is not sufficient for the directed electron transfer process we were aiming for. Further investigation of artificial photoactivation using smaller sized NPs might link directly to the αC158 site and subsequentially provide sufficient electron flux to ungate the nitrogenase electron transfer mechanism. If indeed will be realized, MV will become otiose as a result of the direct electron injection to the P cluster. A great example for that was already shown, while photoreduction of acetylene was performed using $Ru(bpy)_3$ photosensitizer bonded to αL158C MoFe-P.[24]

In conclusion, we examined the photoactivation of nitrogenase by CdS NPs. NPs were modified with TGA acid or ME ligands and their aptness to bind and activate nitrogenase was tested. We show for the first time TEM imaging of the hybrids. We further examined the systems using electrochemical, spectroscopic, and analytical tools. The effect of MV, as a redox mediator, on the generation of ammonia and hydrogen was examined. Our results show that ME-modified NPs have an advantage in hydrogen generation compared with TGA ligands, while a similar amount of ammonia was detected for both configurations. Adding MV led to complete elimination of hydrogen generation, while ammonia amounts increased five-fold. These results improve our understanding of the interface between the nitrogenase enzyme and abiotic materials used for its artificial activation.

Methods

Materials and equipment: All chemicals and solvents used were at least analytical grade and were used as received. UV-Vis spectra were acquired using an Evolution 201 - Thermo Scientific spectrophotometer. Gas samples were analyzed via gas chromatography (GC) using an HP/Agilent 6890 (G1530A) system equipped with a 5-Å column and a thermal conductivity detector. Fluorescence intensity was measured by a plate reader (Synergy H1, BioTek) using a Hellma black quartz microplate. All electrochemical measurements were performed using a Biologic SP200 Potentiostat. TEM measurements were performed using a BioTWIN T12 and zeta potential was measured using a Malvern Zetasizer Ultra setup.

CdS nanoparticle synthesis (10 nm): CdS NPs were synthesized using a previously reported method with some modifications (see TEM images in Figs 1a and S1).[43] 91 mg of cadmium chloride ($CdCl_2$, 99.99%, Sigma-Aldrich), 20 mL of 1-octadecene (ODE, 90%, Sigma-Aldrich), and 1.578 mL oleic acid (OA, Fisher Scientific) were mixed in a 100 mL round bottom flask. While purging the flask with Ar atmosphere, the solution was heated to 120 °C and held for 1 h to remove oxygen and residual water. After 1 h, Ar supply was removed and temperature was raised to 220 °C. In a separate vail, 16 mg sulfur (S, 99.5% Sigma-Aldrich) was mixed with 1.646 mL oleylamine (OLA, 70% Sigma-Aldrich). The solution was purged with Ar for 15 min and heated to 70 °C until sulfur was completely dissolved. The solution was then stored under heating (70 °C) until use. Once the temperature of the ODE mixture reached 220 °C, the sulfur mixture was injected into the ODE solution, allowing 10 min of growth. The resulting CdS solution was quenched in a warm water bath and subsequently cooled to room temperature. The cooled CdS solution was then washed to remove unreacted $CdCl_2$, S, OA, and OLA. The CdS solution (≈10 mL) was then transferred into two 50-mL conical centrifuge tubes and mixed with 5 mL of toluene followed by ≈30 mL of acetone. The CdS NPs solution was then centrifuged (8,000 rpm, 5 min) and the supernatant was discarded. The dry CdS NPs were stored in the dark in a glove box (O_2< 0.2 ppm).

CdS ligand exchange to 2-mercaptoethanol (CdS-ME NPs): A fraction of the dry CdS NPs stock was dissolved in 5 mL of toluene. While stirring vigorous, a separately prepared solution of 5 mL dd-H_2O, 200 μL of ME (>99.0%, Sigma-Aldrich), and 120 μL of 1 M NaOH was added to the CdS/toluene solution. This solution was then vigorously stirred overnight in the dark until the ligand-modified NPs were transferred to the aqueous phase. Upon completion, the colorless toluene phase was discarded and the water-soluble CdS-ME NPs were centrifuged at 200 x g for 2 min to yield a clear, yellow solution (see Fig. S2). This clean solution was then filtered using a 30 kDa centrifuge filter (Amicon Ultra-15, Mercury) at 4,200 rpm to remove any excess ligand. CdS-ME NPs were then re-dissolved in H_2O and their concentration was determined by UV-Vis spectroscopy (excitation coefficient of 2.56×10^6 $M^{-1} \cdot cm^{-1}$ at 472 nm).

CdS ligand exchange to thioglycolic acid (CdS-TGA NPs): TGA (98%, Sigma-Aldrich) was added to a stock solution of CdS-ME NPs until the solution turned hazy (≈5 µL TGA per mL of CdS-ME). The solution was then stirred in the dark for 5 hr following which 1 M NaOH was slowly added until the solution became clear. Upon completion, the CdS-TGA NPs were cleaned using a 30 K centrifuge filter (Pall Corporation) at 4,200 rpm. The CdS-TGA NPs were then re-dissolved in H_2O and the concentration was determined by UV-Vis spectroscopy. CdS-ME to CdS-TGA ligand exchange was also confirmed via agarose gel electrophoresis and zeta potential measurement.

Light-driven NH_3 and H_2 production from nitrogenase: Reaction mixtures were prepared in 1.8 mL glass vials sealed with autosampler screw caps. CdS-ME / TGA NPs - MoFe-P biohybrid mixtures were prepared by mixing 51 mM ascorbic acid (AA, Aldrich), 120 nM CdS-ME / TGA NPs, and 1.7 µM methyl viologen dichloride hydrate (MV, 98%, Sigma-Aldrich) in 0.1 M PB pH-7.2. The solutions were then purged with N_2 for 1 h before 100 µL of 4 µM of MoFe-P was injected into the reaction mixture (VT = 560 µL) in an Ar-atmosphere glovebox (O_2< 0.2 ppm). The biohybrid mixtures were then photoirradiated by a 465 nm LED light at 30 °C with gentle stirring. After 2 hrs, irradiation was stopped and H_2 and NH_3 were quantified.

H_2 quantification: H_2 production was measured by injecting an 80 µL sample from the reaction headspace into a GC-TCD inlet septum equipped with a 5-Å column. H_2 was quantified using the calibration curve presented in Fig. S4.

NH_3 quantification: NH_3 production was determined using an OPA (≥97%, Sigma-Aldrich) as a fluorescence probe.[25,44] 400 µl of the irradiated nano-bio hybrid solution was mixed with 400 µl OPA reagent containing 20 mM OPA, 3.4 mM ME in 0.2 M phosphate buffer (pH 7.0), and 5% ethanol. The samples were incubated for 1 h in the dark at 37 °C. Extraction and concentration of the NH_3/OPA conjugates were performed by adding 200 µl of chloroform while vigorously stirring for 20 sec (Fig. S6). The lower phase (chloroform) was then collected and transferred to a new tube. The extracted NH_3/OPA conjugates was diluted five-fold with chloroform and loaded into a 96-well black quartz plate (Hellma). Fluorescence intensity of the different samples was measured using a plate reader (Synergy H1, BioTek; λ excitation=410 nm, λ emission=472 nm). NH_3 was quantified using the calibration curve shown in Fig. S5.

Acknowledgment:

We thank Prof. Dennis Dean of Virginia-Tech and Prof. Jennifer N. Cha of the University of Colorado, Boulder for sharing the *Azotobacter vinnelenlii* mutated strains DJ1194 and DJ995 and growth methods. We thank the Israel Science Foundation for its financial support (Grant No. 2027676).

References:

(1) O. Saboe, P.; Conte, E.; Farell, M.; C. Bazan, G.; Kumar, M. Biomimetic and Bioinspired Approaches for Wiring Enzymes to Electrode Interfaces. *Energy & Environmental Science* **2017**, *10* (1), 14–42. https://doi.org/10.1039/C6EE02801B.

(2) Ruiz, M. P.; Aragonès, A. C.; Camarero, N.; Vilhena, J. G.; Ortega, M.; Zotti, L. A.; Pérez, R.; Cuevas, J. C.; Gorostiza, P.; Díez-Pérez, I. Bioengineering a Single-Protein Junction. *J. Am. Chem. Soc.* **2017**, *139* (43), 15337–15346. https://doi.org/10.1021/jacs.7b06130.

(3) Fereiro, J. A.; Yu, X.; Pecht, I.; Sheves, M.; Cuevas, J. C.; Cahen, D. Tunneling Explains Efficient Electron Transport via Protein Junctions. *PNAS* **2018**, *115* (20), E4577–E4583. https://doi.org/10.1073/pnas.1719867115.

(4) Willner, B.; Katz, E.; Willner, I. Electrical Contacting of Redox Proteins by Nanotechnological Means. *Current Opinion in Biotechnology* **2006**, *17* (6), 589–596. https://doi.org/10.1016/j.copbio.2006.10.008.

(5) Heller, A. Electrical Wiring of Redox Enzymes. *Acc. Chem. Res.* **1990**, *23* (5), 128–134. https://doi.org/10.1021/ar00173a002.

(6) Boussema, F.; Gross, A. J.; Hmida, F.; Ayed, B.; Majdoub, H.; Cosnier, S.; Maaref, A.; Holzinger, M. Dawson-Type Polyoxometalate Nanoclusters Confined in a Carbon Nanotube Matrix as Efficient Redox Mediators for Enzymatic Glucose Biofuel Cell Anodes and Glucose Biosensors. *Biosensors and Bioelectronics* **2018**, *109*, 20–26. https://doi.org/10.1016/j.bios.2018.02.060.

(7) Algov, I.; Grushka, J.; Zarivach, R.; Alfonta, L. Highly Efficient Flavin–Adenine Dinucleotide Glucose Dehydrogenase Fused to a Minimal Cytochrome C Domain. *J. Am. Chem. Soc.* **2017**, *139* (48), 17217–17220. https://doi.org/10.1021/jacs.7b07011.

(8) Yan, Y.-M.; Baravik, I.; Yehezkeli, O.; Willner, I. Integrated Electrically Contacted Glucose Oxidase/Carbon Nanotube Electrodes for the Bioelectrocatalyzed Detection of Glucose. *J. Phys. Chem. C* **2008**, *112* (46), 17883–17888. https://doi.org/10.1021/jp805637e.

(9) Riedel, M.; Parak, W. J.; Ruff, A.; Schuhmann, W.; Lisdat, F. Light as Trigger for Biocatalysis: Photonic Wiring of Flavin Adenine Dinucleotide-Dependent Glucose Dehydrogenase to Quantum Dot-Sensitized Inverse Opal TiO_2 Architectures via Redox Polymers. *ACS Catal.* **2018**, *8* (6), 5212–5220. https://doi.org/10.1021/acscatal.8b00951.

(10) Zhao, F.; Conzuelo, F.; Hartmann, V.; Li, H.; Nowaczyk, M. M.; Plumeré, N.; Rögner, M.; Schuhmann, W. Light Induced H_2 Evolution from a Biophotocathode Based on Photosystem 1 – Pt Nanoparticles Complexes Integrated in Solvated Redox Polymers Films. *J. Phys. Chem. B* **2015**, *119* (43), 13726–13731. https://doi.org/10.1021/acs.jpcb.5b03511.

(11) Gorka, M.; Schartner, J.; van der Est, A.; Rögner, M.; Golbeck, J. H. Light-Mediated Hydrogen Generation in Photosystem I: Attachment of a Naphthoquinone–Molecular Wire–Pt Nanoparticle to the A_{1A} and A_{1B} Sites. *Biochemistry* **2014**, *53* (14), 2295–2306. https://doi.org/10.1021/bi500104r.

(12) Grimme, R. A.; Lubner, C. E.; Bryant, D. A.; Golbeck, J. H. Photosystem I/Molecular Wire/Metal Nanoparticle Bioconjugates for the Photocatalytic Production of H_2. *J. Am. Chem. Soc.* **2008**, *130* (20), 6308–6309. https://doi.org/10.1021/ja800923y.

(13) Yehezkeli, O.; Tel-Vered, R.; Wasserman, J.; Trifonov, A.; Michaeli, D.; Nechushtai, R.; Willner, I. Integrated Photosystem II-Based Photo-Bioelectrochemical Cells. *Nat Commun* **2012**, *3* (1), 742. https://doi.org/10.1038/ncomms1741.

(14) Reisner, E.; Powell, D. J.; Cavazza, C.; Fontecilla-Camps, J. C.; Armstrong, F. A. Visible Light-Driven H_2 Production by Hydrogenases Attached to Dye-Sensitized TiO_2 Nanoparticles. *J. Am. Chem. Soc.* **2009**, *131* (51), 18457–18466. https://doi.org/10.1021/ja907923r.

(15) Brown, K. A.; Wilker, M. B.; Boehm, M.; Dukovic, G.; King, P. W. Characterization of Photochemical Processes for H_2 Production by CdS Nanorod–[FeFe] Hydrogenase Complexes. *J. Am. Chem. Soc.* **2012**, *134* (12), 5627–5636. https://doi.org/10.1021/ja2116348.

(16) Armstrong, F. A.; Hirst, J. Reversibility and Efficiency in Electrocatalytic Energy Conversion and Lessons from Enzymes. *Proceedings of the National Academy of Sciences* **2011**, *108* (34), 14049–14054. https://doi.org/10.1073/pnas.1103697108.
(17) Hu, Y.; Ribbe, MarkusW. Historic Overview of Nitrogenase Research. In *Nitrogen Fixation*; Ribbe, M. W., Ed.; Methods in Molecular Biology; Humana Press, 2011; pp 3–7. https://doi.org/10.1007/978-1-61779-194-9_1.
(18) Eady, R. R. Structure−Function Relationships of Alternative Nitrogenases. *Chem. Rev.* **1996**, *96* (7), 3013–3030. https://doi.org/10.1021/cr950057h.
(19) Milton, R. D.; Abdellaoui, S.; Khadka, N.; Dean, D. R.; Leech, D.; Seefeldt, L. C.; Minteer, S. D. Nitrogenase Bioelectrocatalysis: Heterogeneous Ammonia and Hydrogen Production by MoFe Protein. *Energy Environ. Sci.* **2016**, *9* (8), 2550–2554. https://doi.org/10.1039/C6EE01432A.
(20) Hu, B.; Harris, D. F.; Dean, D. R.; Liu, T. L.; Yang, Z.-Y.; Seefeldt, L. C. Electrocatalytic CO2 Reduction Catalyzed by Nitrogenase MoFe and FeFe Proteins. *Bioelectrochemistry* **2018**, *120*, 104–109. https://doi.org/10.1016/j.bioelechem.2017.12.002.
(21) Milton, R. D.; Cai, R.; Abdellaoui, S.; Leech, D.; De Lacey, A. L.; Pita, M.; Minteer, S. D. Bioelectrochemical Haber–Bosch Process: An Ammonia-Producing H2/N2 Fuel Cell. *Angew. Chem. Int. Ed.* **2017**, *56* (10), 2680–2683. https://doi.org/10.1002/anie.201612500.
(22) Fourmond, V.; Léger, C. Dinitrogen Reduction: Interfacing the Enzyme Nitrogenase with Electrodes. *Angewandte Chemie International Edition* **2017**, *56* (16), 4388–4390. https://doi.org/10.1002/anie.201701179.
(23) Lee, C. C.; Hu, Y.; Ribbe, M. W. ATP-Independent Formation of Hydrocarbons Catalyzed by Isolated Nitrogenase Cofactors. *Angew. Chem. Int. Ed.* **2012**, *51* (8), 1947–1949. https://doi.org/10.1002/anie.201108916.
(24) Roth, L. E.; Nguyen, J. C.; Tezcan, F. A. ATP- and Iron−Protein-Independent Activation of Nitrogenase Catalysis by Light. *J. Am. Chem. Soc.* **2010**, *132* (39), 13672–13674. https://doi.org/10.1021/ja1071866.
(25) Brown, K. A.; Harris, D. F.; Wilker, M. B.; Rasmussen, A.; Khadka, N.; Hamby, H.; Keable, S.; Dukovic, G.; Peters, J. W.; Seefeldt, L. C.; King, P. W. Light-Driven Dinitrogen Reduction Catalyzed by a CdS:Nitrogenase MoFe Protein Biohybrid. *Science* **2016**, *352* (6284), 448–450. https://doi.org/10.1126/science.aaf2091.
(26) Harris, A. W.; Harguindey, A.; Patalano, R. E.; Roy, S.; Yehezkeli, O.; Goodwin, A. P.; Cha, J. N. Investigating Protein–Nanocrystal Interactions for Photodriven Activity. *ACS Appl. Bio Mater.* **2020**, *3* (2), 1026–1035. https://doi.org/10.1021/acsabm.9b01025.
(27) Hoffman, B. M.; Lukoyanov, D.; Yang, Z.-Y.; Dean, D. R.; Seefeldt, L. C. Mechanism of Nitrogen Fixation by Nitrogenase: The Next Stage. *Chem. Rev.* **2014**, *114* (8), 4041–4062. https://doi.org/10.1021/cr400641x.
(28) Seefeldt, L. C.; Hoffman, B. M.; Dean, D. R. Mechanism of Mo-Dependent Nitrogenase. *Annu Rev Biochem* **2009**, *78*, 701. https://doi.org/10.1146/annurev.biochem.78.070907.103812.
(29) Burgess, B. K.; Jacobs, D. B.; Stiefel, E. I. Large-Scale Purification of High Activity Azotobacter Vinelandii Nitrogenase. *Biochimica et Biophysica Acta (BBA) - Enzymology* **1980**, *614* (1), 196–209. https://doi.org/10.1016/0005-2744(80)90180-1.
(30) Christiansen, J.; Goodwin, P. J.; Lanzilotta, W. N.; Seefeldt, L. C.; Dean, D. R. Catalytic and Biophysical Properties of a Nitrogenase Apo-MoFe Protein Produced by a NifB-Deletion Mutant of Azotobacter Vinelandii. *Biochemistry* **1998**, *37* (36), 12611–12623. https://doi.org/10.1021/bi981165b.
(31) Saruyama, M.; So, Y.-G.; Kimoto, K.; Taguchi, S.; Kanemitsu, Y.; Teranishi, T. Spontaneous Formation of Wurzite-CdS/Zinc Blende-CdTe Heterodimers through a Partial Anion Exchange Reaction. *J. Am. Chem. Soc.* **2011**, *133* (44), 17598–17601. https://doi.org/10.1021/ja2078224.
(32) Wuister, S. F.; de Mello Donegá, C.; Meijerink, A. Influence of Thiol Capping on the Exciton Luminescence and Decay Kinetics of CdTe and CdSe Quantum Dots. *J. Phys. Chem. B* **2004**, *108* (45), 17393–17397. https://doi.org/10.1021/jp047078c.

(33) Lenngren, N.; Abdellah, M. A.; Zheng, K.; Al-Marri, M. J.; Zigmantas, D.; Žídek, K.; Pullerits, T. Hot Electron and Hole Dynamics in Thiol-Capped CdSe Quantum Dots Revealed by 2D Electronic Spectroscopy. *Phys. Chem. Chem. Phys.* **2016**, *18* (37), 26199–26204. https://doi.org/10.1039/C6CP04190F.
(34) Hines, D. A.; Kamat, P. V. Quantum Dot Surface Chemistry: Ligand Effects and Electron Transfer Reactions. *J. Phys. Chem. C* **2013**, *117* (27), 14418–14426. https://doi.org/10.1021/jp404031s.
(35) An, X.; Yu, X.; Yu, J. C.; Zhang, G. CdS Nanorods/Reduced Graphene Oxide Nanocomposites for Photocatalysis and Electrochemical Sensing. *J. Mater. Chem. A* **2013**, *1* (16), 5158. https://doi.org/10.1039/c3ta00029j.
(36) Kumari, S.; Chaudhary, Y. S.; Agnihotry, S. A.; Tripathi, C.; Verma, A.; Chauhan, D.; Shrivastav, R.; Dass, S.; Satsangi, V. R. A Photoelectrochemical Study of Nanostructured Cd-Doped Titanium Oxide. *International Journal of Hydrogen Energy* **2007**, *32* (9), 1299–1302. https://doi.org/10.1016/j.ijhydene.2006.07.017.
(37) Quan, D.; Shin, W. A Nitrite Biosensor Based on Co-Immobilization of Nitrite Reductase and Viologen-Modified Chitosan on a Glassy Carbon Electrode. *Sensors (Basel)* **2010**, *10* (6), 6241–6256. https://doi.org/10.3390/s100606241.
(38) Tagliazucchi, M.; Tice, D. B.; Sweeney, C. M.; Morris-Cohen, A. J.; Weiss, E. A. Ligand-Controlled Rates of Photoinduced Electron Transfer in Hybrid CdSe Nanocrystal/Poly(Viologen) Films. *ACS Nano* **2011**, *5* (12), 9907–9917. https://doi.org/10.1021/nn203683s.
(39) Peterson, M. D.; Jensen, S. C.; Weinberg, D. J.; Weiss, E. A. Mechanisms for Adsorption of Methyl Viologen on CdS Quantum Dots. *ACS Nano* **2014**, *8* (3), 2826–2837. https://doi.org/10.1021/nn406651a.
(40) Owens, C. P.; Katz, F. E. H.; Carter, C. H.; Luca, M. A.; Tezcan, F. A. Evidence for Functionally Relevant Encounter Complexes in Nitrogenase Catalysis. *J. Am. Chem. Soc.* **2015**, *137* (39), 12704–12712. https://doi.org/10.1021/jacs.5b08310.
(41) Owens, C. P.; Tezcan, F. A. Chapter Twelve - Conformationally Gated Electron Transfer in Nitrogenase. Isolation, Purification, and Characterization of Nitrogenase From Gluconacetobacter Diazotrophicus. In *Methods in Enzymology*; David, S. S., Ed.; Fe-S Cluster Enzymes Part B; Academic Press, 2018; Vol. 599, pp 355–386. https://doi.org/10.1016/bs.mie.2017.09.007.
(42) Rutledge, H. L.; Tezcan, F. A. Electron Transfer in Nitrogenase. *Chem. Rev.* **2020**. https://doi.org/10.1021/acs.chemrev.9b00663.
(43) Saruyama, M.; So, Y.-G.; Kimoto, K.; Taguchi, S.; Kanemitsu, Y.; Teranishi, T. Spontaneous Formation of Wurzite-CdS/Zinc Blende-CdTe Heterodimers through a Partial Anion Exchange Reaction. *J. Am. Chem. Soc.* **2011**, *133* (44), 17598–17601. https://doi.org/10.1021/ja2078224.
(44) Corbin, J. L. Liquid Chromatographic-Fluorescence Determination of Ammonia from Nitrogenase Reactions: A 2-Min Assay. *Appl Environ Microbiol* **1984**, *47* (5), 1027–1030.

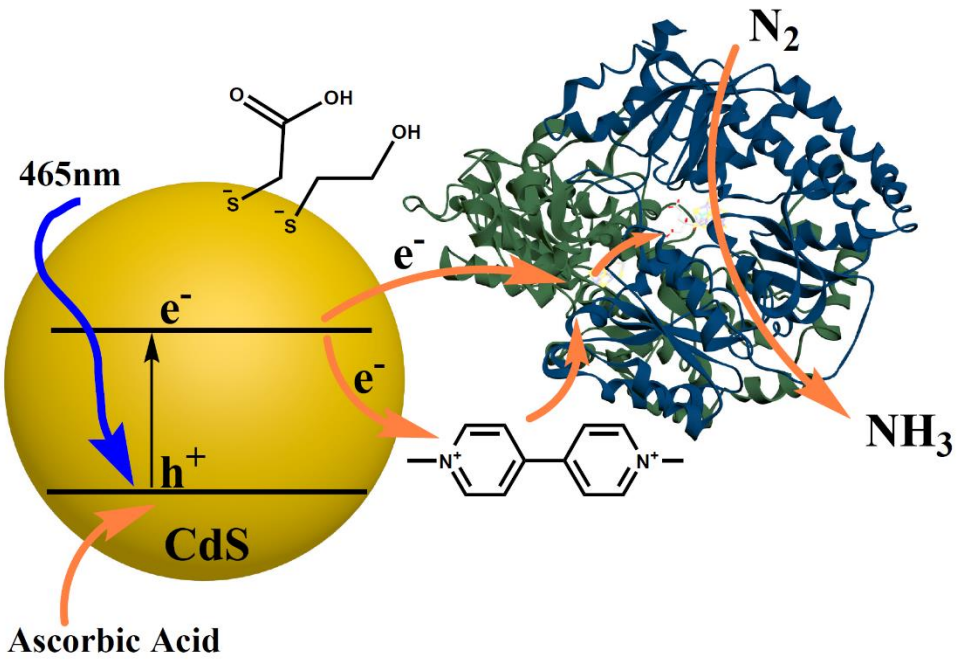

Figure 1: *Schematic of the Photo Bio-Nano-Hybrid systems based on CdS NPs with different ligands (ME / TGA), viologen as redox active mediator and Nitrogenase (MoFe-P).*

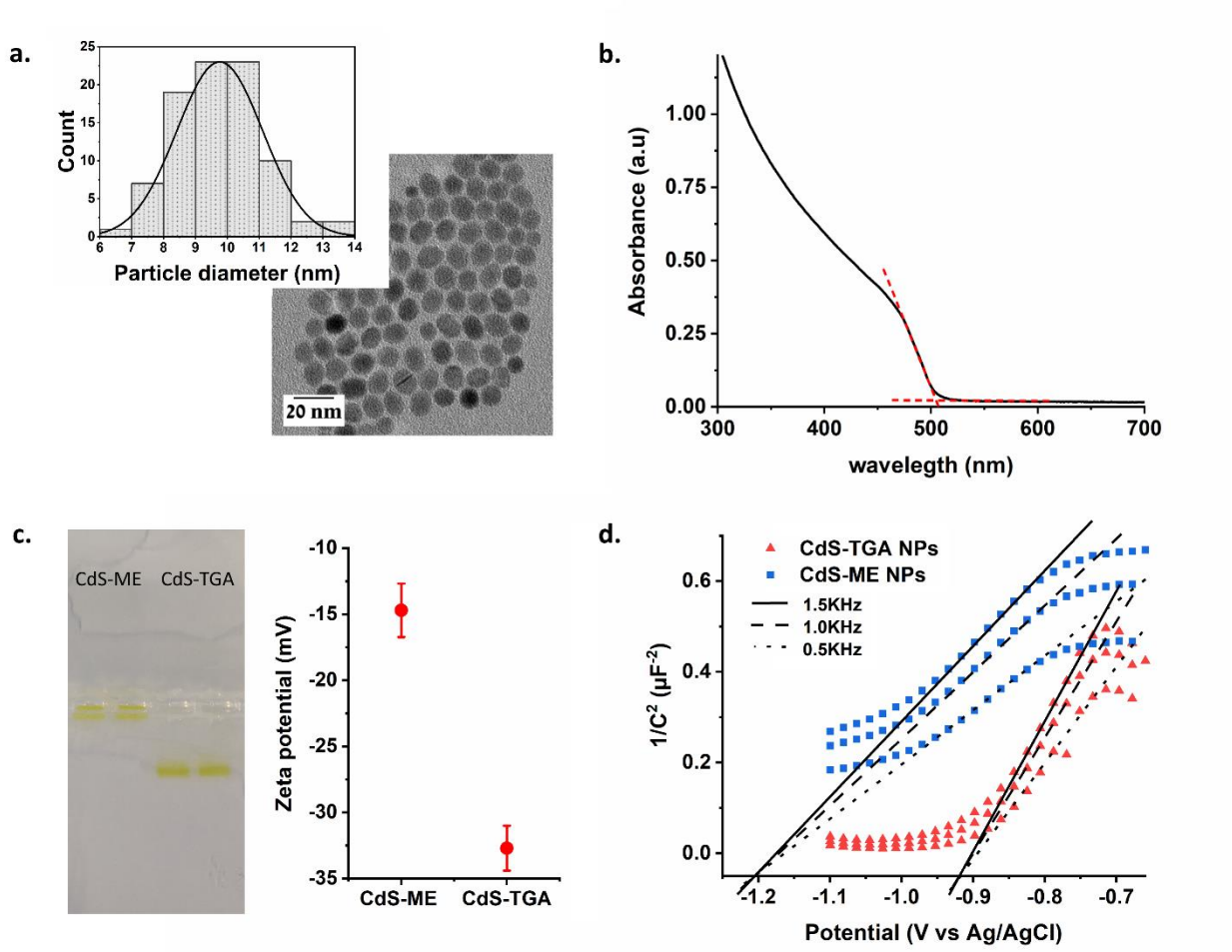

Figure 2: *(a) TEM images of 10nm CdS-ME NPs. Inst. CdS NPs size distribution, (b) UV-Vis absorbance of the 10nm CdS NPs, (c) Agarose gel (0.6%) of CdS-ME / TGA NPs (1.4 μM) and zeta potential of CdS-ME / TGA NPs (120 nM) in 0.1M PB and 51mM AA at pH 7.2, (d) Mott–Schottky plots of CdS-ME / TGA NPs in 0.2 M K_2SO_4 aqueous solution (pH = 7.2). NPs were deposited on glassy carbon electrode.*

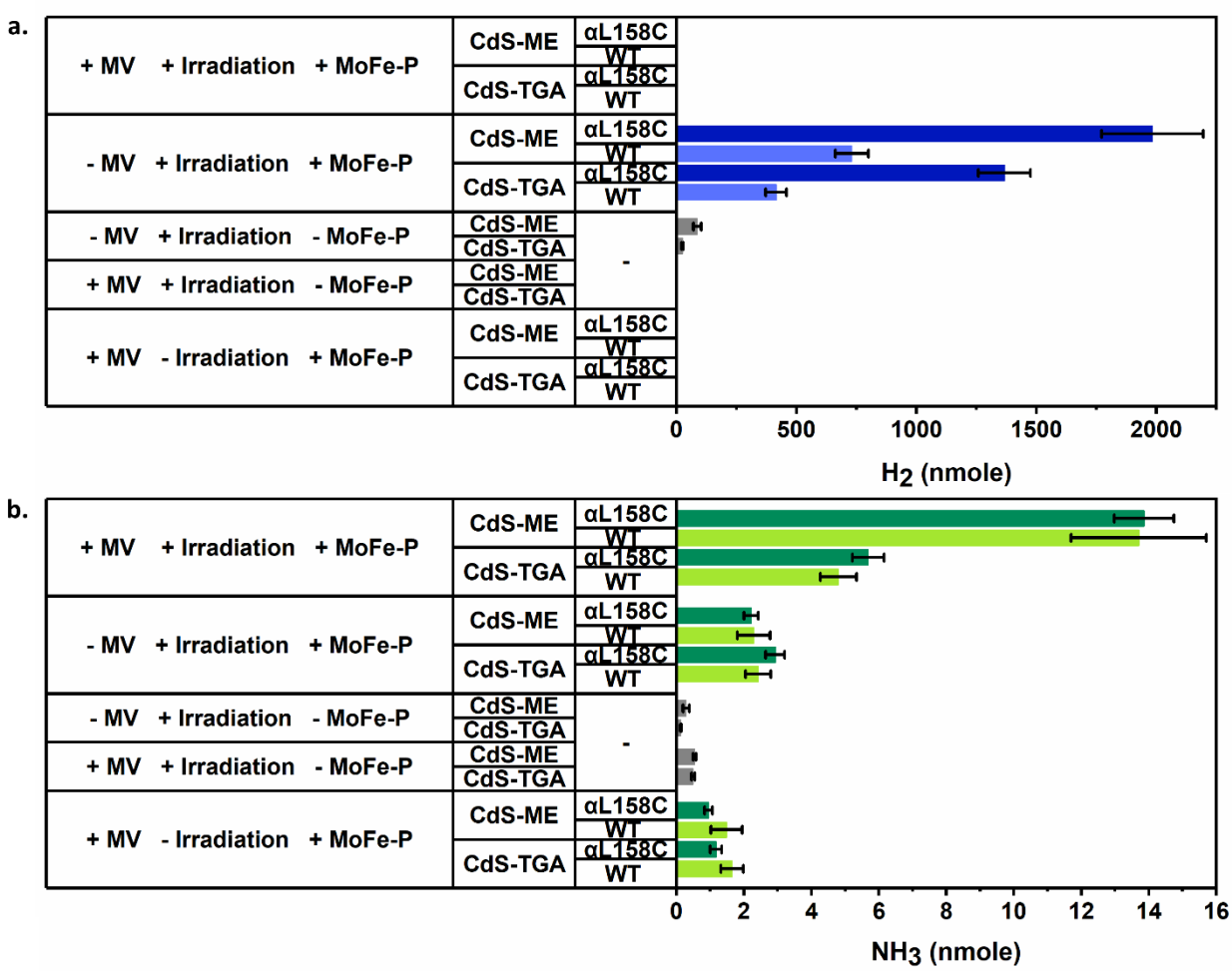

Figure 3: *(a) NH_3 and (b) H_2 production of mediated and non-mediated CdS-ME / TGA NPs: MoFe-P biohybrid systems in 0.1M PB pH 7.2 and 51mM AA after 2hr of irradiation.*

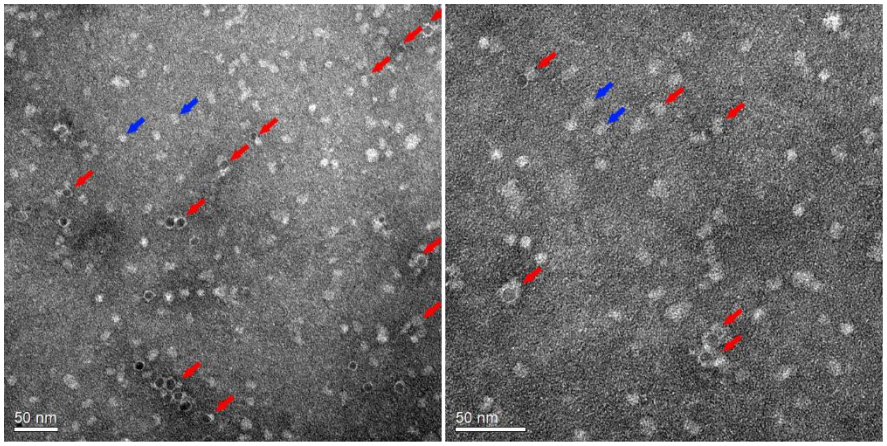

Figure 4: *TEM images of CdS-ME NPs : αL158C MoFe-P biohybrid systems (red arrows). The blue arrows indicate non-absorbed αL158C MoFe-P. Glow discharging was performed for carbon-coated grids and samples were stained with uranyl acetate (1%).*